Biosensors and Bioelectronics 32 (2012) 118–126

Contents lists available at SciVerse ScienceDirect

Biosensors and Bioelectronics

journal homepage: www.elsevier.com/locate/bios

Layer-by-layer self-assembly of functionalized graphene nanoplates for glucose sensing *in vivo* integrated with on-line microdialysis system

Hui Gu[a], Yanyan Yu[a], Xiaoqian Liu[a], Bing Ni[b], Tianshu Zhou[c], Guoyue Shi[a,*]

[a] *Department of Chemistry and Shanghai Key Laboratory of Green Chemistry and Chemical Process, East China Normal University; 3663 Zhongshan Road(N), Shanghai, 200062, PR China*
[b] *Department of Life Science, East China Normal University; 3663 Zhongshan Road (N), Shanghai, 200062, PR China*
[c] *Department of Environmental Science, East China Normal University; 3663 Zhongshan Road(N), Shanghai, 200062, PR China*

ARTICLE INFO

Article history:
Received 4 October 2011
Received in revised form
25 November 2011
Accepted 25 November 2011
Available online 17 December 2011

Keywords:
{IL-RGO/S-RGO}$_n$
Functionalized graphene
On-line microdialysis system
Glucose biosensor
In vivo

ABSTRACT

In this work, a novel amperometric biosensor for hydrogen peroxide was fabricated through the layer-by-layer (LBL) self-assembling of amine-terminated ionic liquid (IL-NH_2), and sulfonic acid (SO_3^-) functionalized graphene by covalent bonding. The modification of the two functionalities introduced positive and negative charge onto the surface of graphene respectively, thus facilitating the formation of a multilayer film denoted with {IL-RGO/S-RGO}$_n$ through electrostatic interaction and further immobilization of glucose oxidase (GOx). The resulting {IL-RGO/S-RGO}$_n$/GOx/Nafion biosensor displayed an excellent response to glucose at a potential of −200 mV. Combined with on-line microdialysis system, the glucose biosensor in the on-line system showed good linear range from 10 μM to 500 μM with the detection limit of 3.33 μM (S/N = 3). Consequently, the basal level of glucose in the striatum of anesthetic rats was calculated to be 0.376 ± 0.028 mM (mean ± s.d., n = 3). The {IL-RGO/S-RGO}$_n$/GOx/Nafion biosensor was further applied for *in vivo* sensing of the glucose level in the striatum when rats received intraperitoneal (i.p.) injection of 30 μL insulin, which resulted in an obvious decrease in the extracellular concentration of glucose within 30 min. The method was proved to be sensitive and reproducible, which enabled its promising application in physiology and pathology.

1. Introduction

Graphene, a counterpart of graphite with well separated 2-D aromatic sheets composed of sp^2-bonded carbon atoms, has attracted extensive interest since its discovery in 2004 (Muszynski et al., 2008). Due to its unique properties, such as high surface area, high electrical conductivity, exceptional thermal properties and strong mechanical strength (Stankovich et al., 2006a,b; Lee et al., 2008; Zeng et al., 2010), immense interest has been indeed spurred in designing novel graphene-based materials for a variety of technological applications such as nanoelectronics, biosensing, electromechanical resonators, H_2 production and storage, batteries, biofuel cells, drug delivery and catalysis (Allen et al., 2010; Stoller et al., 2008; Subbiah et al., 2010; Guo et al., 2010; Stankovich et al., 2006a,b; Zhang et al., 2010). To produce single- or few- or multi-layered graphene nanosheets, various approaches have been established which include chemical vapor deposition (CVD) of methane gas (Reina et al., 2009; Li et al., 2009), graphite oxide reduction (Tung et al., 2009), carbon nanotube unzipping (Kosynkin et al., 2009), and epitaxial growth of graphene resulted from the high temperature reduction of silicon carbide (Berger et al., 2006). Among them, chemical conversion from graphite powder to graphite oxide (GO) and further reduction to graphene is more attractive due to its economic feasibility and massive scalability.

However, these unique properties are associated with individual sheets, which put forwards the importance of surmounting its inherent disadvantages, such as hydrophobicity and easy-to-aggregation in aqueous solution. This challenge of obtaining well-dispersed graphene has been well addressed through covalent and uncovalent functionalization methods. Xu et al. have synthesized uncovalent functionalized graphene with a water-soluble pyrene derivative, 1-pyrenebutyrate (PB-) (Xu et al., 2008). An et al. have reported the graphene has been achieved by noncovalent functionalization of graphene with 1-pyrenecarboxylic acid in a polarity-controlled combination (An et al., 2010). Graphene has been covalent modified with a long-chain alkylamine by Niyogi et al. (2006) group. Shan's group has presented functionalization of graphene with biocompatible poly-L-lysine as a linker through a covalent amide group (Shan et al., 2009). However, noncovalent

Abbreviations: LBL, layer-by-layer; IL-NH_2, amine-terminated ionic liquid; SO_3^-, sulfonic acid; S-RGO, sulfonic acid (SO_3^-) functionalized graphene; IL-RGO, amine-terminated ionic liquid functionalized graphene; Gox, Glucose oxidase; AA, ascorbic acid; DA, dopamine; UA, uric acid.

* Corresponding author. Tel.: +82 31 3290 4853; fax: +82 2 926 6102.
E-mail addresses: gyshi@chem.ecnu.edu.cn, iamshgy@hotmail.com (G. Shi).

0956-5663/$ – see front matter © 2011 Elsevier B.V. All rights reserved.
doi:10.1016/j.bios.2011.11.044

functionalization of graphene sheets is through π–π interactions and vander Waals interaction, which is less stable compared with the covalent modified graphene through covalent interactions (Liu et al., 2009; Xu et al., 2008; Shan et al., 2009). Our methodology introduces sulfonic acid groups and the amine-terminated ionic liquid (IL-NH_2) in graphene in a simple way (Yang et al., 2009a,b; Si et al., 2008). The charged -SO_3^- units prevent the graphitic sheets from aggregating in solution after the final reduction stage of the graphene oxide, thereby yielding isolated sheets of lightly sulfonated graphene with improved water solubility. The cations of IL-NH_2 contribute to a well dispersible graphene-based material with good stabilization *via* electrostatic repulsion. Consequently, it makes it a possible route to harnessing excellent properties of graphene sheets for applications through incorporating them into composite materials (Kosynkin et al., 2009).

Recently, considerable efforts have been made to fabricate different graphene-based nanocomposites and explore their applications in various fields (Zhang et al., 2011; Bai et al., 2011). Layer-by-layer assembly method is of intrinsical advantages to assemble ultrathin films of a variety of organic and inorganic compounds in a simple and inexpensive manner, with thickness controllable in the nanometer range (Zhu and Tour, 2010). However, the formation of graphene-based LBL films has been much less discussed in the literature, especially fabrication of the two carbon-based nanomaterials (Kong et al., 2009; Yu and Dai, 2010). Herein, to fabricate the chemically self-assembled graphene thin films, the positively charged IL-RGO are alternately complexed with the negatively charged S-RGO through an electrostatic LBL process. Simply by varying the number of LBL depositions, the physical properties of the constructed thin films, such as film thickness or optical transparency, can be readily manipulated (Park et al., 2011).

In this work, a simply sequential immersion method was employed to fabricate a novel biosensor by {IL-RGO/S-RGO}$_n$ composite material, whose unusually electronic properties make it suitable for electrochemical sensing. The modified procedure was shown in Scheme 1 (supporting information). Except to overcome the unsatisfying hydrophobicity of pure graphene, the IL-RGO/S-RGO films can not only enhance the electrochemical response with its good ionic conductivity, but also sustain most of the continuous π-electronic structure of graphene sheets and introduce a positive and negative charge in aqueous solution, which realized the immobilization of glucose oxidase *via* electrostatic interaction under mild conditions. Herein, we also demonstrated an excellent electrocatalytic activity toward H_2O_2 at {IL-RGO/S-RGO}$_n$ modified electrode. What is more, a third generation glucose biosensor based upon {IL-RGO/S-RGO}$_n$ films was constructed with GOx as the biological recognition element. Because of the synergetic affects of the two conductive graphenes, the direct electron transfer can be efficiently achieved between electrode surface and the immobilized GOx. The mediatorless on-line detection of glucose was realized continuously at a potential of −200 mV in the striatum of rat with on-line microdialysis system. The construction of on-line microdialysis system and the performance of the glucose biosensor with respect to sensitivity, selectivity and the detection limit *etc.* were presented and discussed in this work. Finally, the prepared biosensor was applied to monitor the variation of glucose concentration in rat's striatum stimulated by intraperitoneal (i.p.) injection of 30 μL insulin injection.

2. Experimental

2.1. Materials

Graphite powder (GO, 99.5%, 325 mesh) and 1-Methylimidazole (>99%) were purchased from TCI Development Co., Ltd (Shanghai, China). 2-Bromoethylamine hydrobromide (99%) and Hydrazine solution (85%) were obtained from Shanghai Darui Finechemical Co., Ltd (Shanghai, China). Unless otherwise stated, other reagents were of at least analytical grade and used as received. All aqueous solutions were prepared with distilled water.

2.2. Fabrication of {IL-RGO/S-RGO}$_n$/GOx/Nafion biosensor through layer-by-layer self-assembly

The glassy carbon (3-mm diameter, CHI Company) electrode (GCE) was used in both off-line and on-line electrochemical experiments. Prior to surface modification, the GC electrode was polished with 0.05 μm alumina followed by successive sonication in acetone, HNO_3 (1:1, v/v), NaOH (50%, w/w) and pure distilled water. Afterward, the clean GCE was immersed into IL-RGO dispersion (5 mg/mL) for 30 min to adsorb a positively charged layer, then, washed with distilled water and dried under ambient condition. The IL-RGO modified electrode was sequentially immersed into the prepared anionic S-RGO dispersion (2 mg/mL) for 30 min again, on which a negatively charged film was adsorbed onto the IL-RGO-GCE, followed by the same washing and drying procedure. This affords one bilayer of IL-RGO and S-RGO with a notation of {IL-RGO/S-RGO}$_1$. Multilayer films were fabricated by alternating the deposition between IL-RGO and S-RGO until desired number of bilayers was achieved. For co-fabrication of glucose oxide (GOx) onto the surface of (IL-RGO/S-RGO)$_n$, an additional immersion in the IL-RGO suspension was firstly performed to introduce the positive charge. After drying and washing, it was then soaked in 10 mg/mL GOx solution (0.1 M phosphate-buffered saline, pH 7.4) for 24 h at 4 °C. At this pH, GOx (pI = 4.5) bears a net negative charge, thus allowing electrostatic attraction with positively charged IL-RGO film. Finally, a thin film of 0.5% Nafion solution was coated. The resulting {IL-RGO/S-RGO}$_n$/GOx/Nafion electrode was stored at 4 °C when not in use.

2.3. Animal experiments

All procedures involving animals were conducted with the approval of the Animal Ethics Committee in ECNU, China. Male Sprague–Dawley rats (weight ranges from 200 to 250 g) were purchased from Shanghai SLAC Laboratory animal Co. Ltd and acclimatized for 4 days. Then the rats were anesthetized with chloral hydrate (initial dose of 300 mg/kg (i.p.) with additional doses of 50 mg/kg (i.p.) as needed to maintain anesthesia) and wrapped in a homeothermic blanket (Beijing Tide-Gene Biotechnology Development Center). The rats were placed in a stereotaxic frame (Beijing Tide-Gene Biotechnology Development Center) with the incisor bar set at 5 mm above the interaural line and appropriately placed holes were drilled through the skull. The microdialysis probe (CMA/110/111 Tub) was implanted in the striatum at the site of 2.5 mm anterior to bregma, 2.5 mm lateral from midline, and 7.0 mm below dura. In order to reduce the injury to the rat, the microdialysis probe should be implanted into the striatum of rats slowly within 30 min with special care.

2.4. In vivo experimental design

The *in vivo* experiment was performed as previously reported (Shi et al., 2003; Yu et al., 2011a,b). Firstly, aCSF solution in one syringe was pumped into the on-line microdialysis system at 2.0 μL/min and flowed to the thin-layer electrochemical flow cell. After a stable baseline was achieved, the syringe selector was then switched to another syringe. The current started to increase slowly and reached a plateau within several minutes, which was ascribed to the biosensing of glucose in the striatum of rat. At last, 30 μL

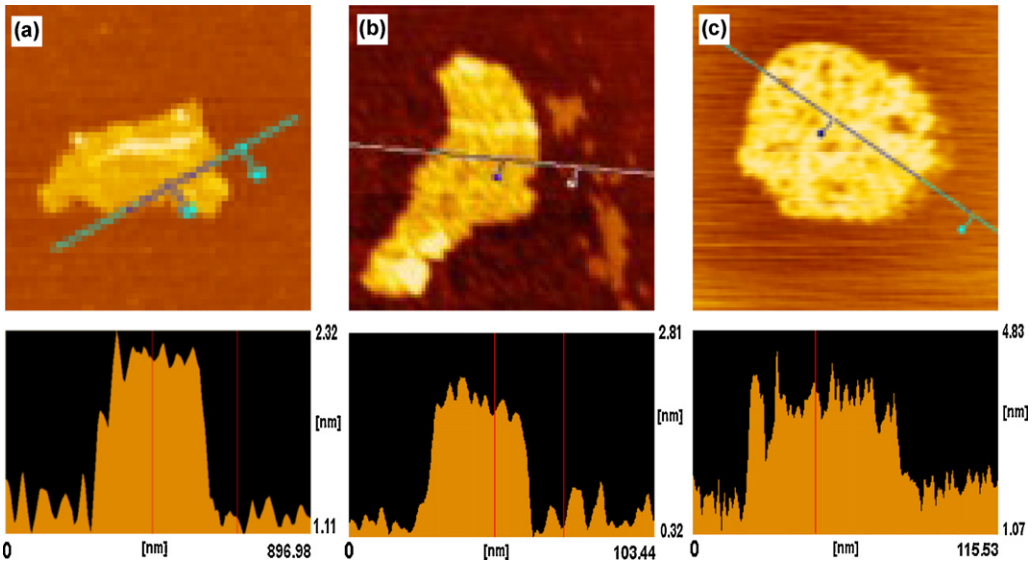

Fig. 1. AFM image of images of GO (a), S-RGO (b), IL-RGO (c) on a Si/SiO_2 wafer through drop-casting, and height profiles along the line shown in AFM image.

insulin was intraperitoneally injected into the rat and the variation of glucose was investigated.

Before on-line electrochemical measurements, the microdialysis probes were implanted into the striatum of rats and perfused with aCSF solution at 2.0 μL/min for at least 90 min for equilibration and the injury recovery. The on-line electrochemical biosensor was calibrated with standard solutions of glucose before and after on-line measurements to ensure there is no obvious change in the sensitivity after the measurements of the brain microdialysis.

2.5. Statistical analysis

Basal level and variation of glucose concentration after insulin intraperitoneally injection in the striatum of rats *in vivo* were expressed as absolute concentrations. Three rats at least were employed for both normal and stimulation experiments. All data were presented as mean ± S.D. ($n = 3$).

3. Results and discussion

3.1. Characteristics of GO, S-RGO and IL-RGO

Fig. 1 shows the typical atomic force microscope (AFM) images of GO (a), S-RGO (b) and IL-RGO (c). Height profiles along the line show that the thickness of GO (a) is about 0.95 nm, which is characteristics of fully exfoliated graphene sheets, consistent with previous literatures (Zhou et al., 2009; Li et al., 2008; Si et al., 2008; Yang et al., 2009a,b). Moreover, the larger thickness of 1.36 and 1.59 nm for S-RGO (b) and IL-RGO (c) respectively in comparison with pure graphene verifies the successful modification of the $-SO_3$ and IL-NH_2 onto graphene sheets. It is also worthwhile to note that the lateral dimensions of GO (a), S-RGO (b) and IL-RGO (c) are more than 1 μm. which are well agreed with the observations in the TEM images (Fig. 2).

Fig. 2a–c show transmission electron microscope (TEM) images of the GO (a), S-RGO (b) and IL-RGO (c) transferred onto holey carbon grids. We can see that the GO has a typical shape resembling the large crumpled thin flake, and the S-RGO (b) and IL-RGO (c) do not change significantly after functionalization from the morphologies. The wrinkles on the graphene sheets are clearly observed. These wrinkles may be important for preventing aggregation of graphene due to van der Waals forces during drying and maintaining high surface area (Kou et al., 2009). Fig. 2d–f show Scanning Electron Microscope (SEM) of GO (d), S-RGO (e) and IL-RGO (f). Compared with GO (Fig. 2d), the morphology of S-RGO (Fig. 2e) is not greatly changed, but the image of the IL-RGO (Fig. 2f) is distinguishable from the GO by its appearance of seemly being cover a layer of jelly, which maybe stem of the attachment of IL-NH_2 units to GO nanosheets.

FTIR spectroscopy was also performed to further confirm the reaction between the sulfonic acid group, IL-NH_2 and GO shown in Fig. 3A. The peaks at 1362 cm^{-1} and 1280 cm^{-1} in curve (a) correspond to the skeletal vibrations of C—OH and C—O—C in unoxidized graphitic domains (Stankovich et al., 2006a,b; Si et al., 2008), and C═O and C—O stretching vibration bands of COOH groups are at 1735 cm^{-1} and 1055 cm^{-1} (Liu et al., 2010). The resonance at 1623 cm^{-1} can be assigned to the vibrations of the adsorbed water molecules, but may also contain components from the skeletal vibrations of un-oxidized graphitic domains (Szabo and Berkesi, 2005; Cataldo, 2003). The typical peaks at 1163 cm^{-1}, 1100 cm^{-1}, and 1030 cm^{-1} (two ν_{s-o} and one $\nu_{s\text{-phenyl}}$) in Fig. 3A (b) confirm the presence of sulfonic acid groups, and the peaks at 997 cm^{-1} (νs-C—H in-plane bending) and 827 cm^{-1} (out-of-plane hydrogen wagging) are characteristic vibrations of p-disubstituted phenyl groups. Meanwhile, the absence of the peaks at 1365 cm^{-1} and 1250 cm^{-1} indicates the epoxide and the hydroxyl groups attached to the basal graphene layer have been removed, which corroborates the reduction of the S-RGO. As shown in Fig. 3A (c), the peaks at 2851 cm^{-1} and 2924 cm^{-1} correspond to symmetric vs(CH_2) and asymmetric vas(CH_2) of the IL-NH_2 units which have been grafted on the GO nanosheets basal plane, and the peak of the 1163 cm^{-1} may be from the CH_3 (N) stretching, CH_2 (N) stretching, and ring in-plane asymmetric stretching arising from imidazolium ring (Yang et al., 2009a,b), which further corroborates the successful attachment of IL-NH_2 units to GO nanosheets.

To further illustrate the covalent functionalization, X-ray photoelectron spectroscopy (XPS) was performed on GO (Fig. 3B (a), (b)), IL-RGO (Fig. 3B(c) and (d)) and S-RGO (Fig. 3B(e)–(g)). The survey XPS analysis of IL-RGO (Fig. 3B(c)) on a Si wafer shows an absence of any detectable amounts of K19 (the strongest XPS band is K2p, usually found between 290 and 297 eV) and any detectable amounts of Br (the strongest XPS band is Br3d, usually found between 65 and 85 eV), indicating that the catalyst has been removed efficiently and the Br anions may have been exchanged by hydroxyl anions. As shown in Fig. 3B(c), the N1s band appears at 401.7 eV, confirming the presence of IL-NH_2 units in IL-RGO, in accordance with the

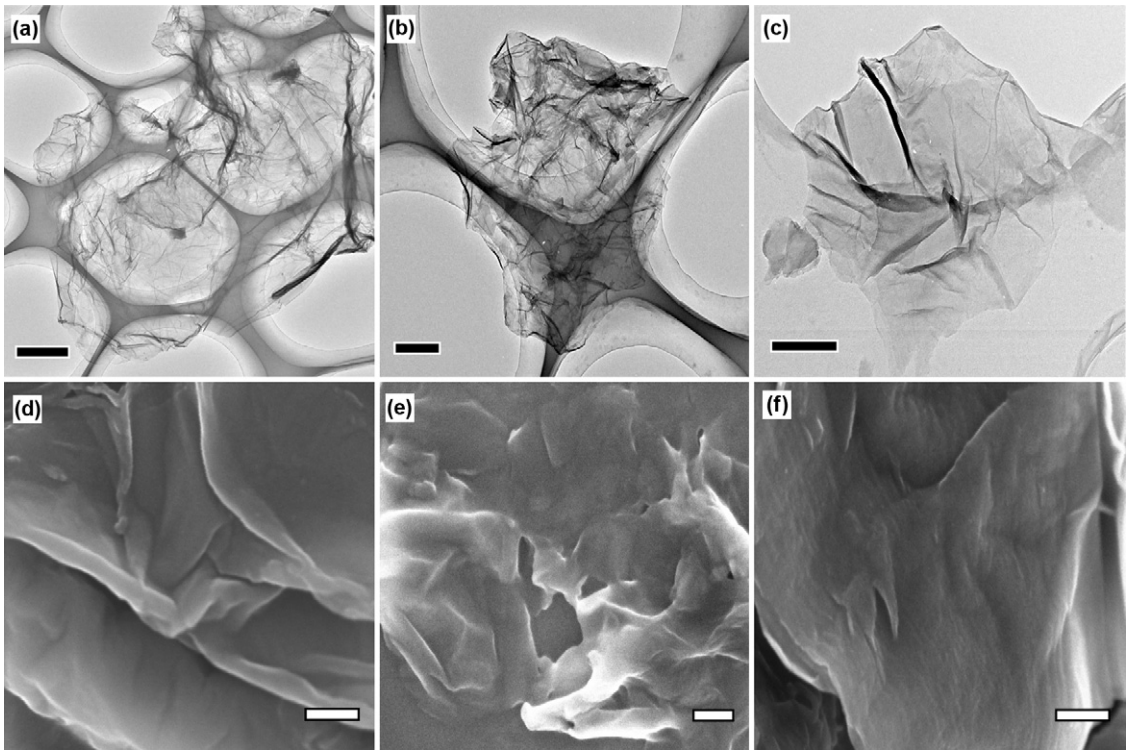

Fig. 2. Typical TEM of GO (a), S-RGO (b), IL-RGO (c), All scale bars shown represent 500 nm. Typical SEM of GO (d), S-RGO (e), IL-RGO (f), All scale bars shown represent 100 nm.

FTIR results (Fig. 2). The C1s XPS spectrum of GO (Fig. 3B(a) and (b)) clearly indicates a certain degree of oxidation, with four different components corresponding to carbon atoms in different functional groups: C-C in graphite, in C–OH, in C–O (epoxy/ether) groups, and the carbonyl C. Although the C1 s XPS spectrum of IL-RGO (Fig. 3B (d)) also exhibits the same oxygen functional groups, a decreased amount of C in epoxy/ether groups is clearly observed. There is also an additional component at 285.9 eV, which accompanies the decrease in epoxy groups, and the new component can be assigned to the combination of the C bound to nitrogen which newly appears after reaction and the C—N groups from the imidazolium ring of the ionic liquid. These results taken together indicate that the covalent reaction between amino moieties of IL-NH_2 and the epoxy groups on GO sheets occurred successfully. The survey XPS analysis of S-RGO (Fig. 3B (e)) on a Si wafer shows an absence of any detectable amounts of N7, (the strongest XPS band is N1s, usually found between 395 and 405 eV) indicating that the hydrazine has been removed efficiently and that diazonium salt has been successfully functionalized onto the surface of the graphene. As can be seen from Fig. 3B (g), high-resolution XPS S 2p of S-RGO shows evidence of a sulfonic group, in accordance with the FTIR results (Fig. 3A). Although the C1s XPS spectrum of IL-RGO (Fig. 3B(d)) and S-RGO (Fig. 3B(f)) also exhibits the same oxygen functional groups, the GO, used in function reaction in this work, has not reach the extent of Highly oxidation, which result that the oxygen-containing groups on GO cannot be significantly removed in the following function reaction.

3.2. Layer-by-layer self-assembly of IL-RGO and S-RGO

Fig. 4 presents the SEM characterization of the $\{$IL-RGO/S-RGO$\}_n$ films following one layer (a), three layers (b) and five layers (c) coating. It can be clearly observed that after the first layer modification, certain amount of graphene sheets has been coated on ITO surface (Fig. 4a), indicating the successful deposition of graphene sheets on the substrate. With the increasing number of bilayers, the surface density of graphene sheets also increases. After five deposition cycles (Fig. 4c), graphene sheets have densely covered on the substrate. To further evaluate the growth process of the $\{$IL-RGO/S-RGO$\}_n$ multilayer films, UV–vis spectroscopy, which has proved to be a useful and facile technique to monitor the LBL self-assembly process of $\{$IL-RGO/S-RGO$\}_n$ multilayer films, was also employed in this work. As can be seen, with the number of bilayer increases, the adsorption peak at 310 nm, gradually grows in intensity, which indicates the successful deposition of graphene on ITO surface and thus, the absorption peak at 310 nm can be utilized to determine the graphene of the multilayer in a given bilayer. Furthermore, the absorption peak at 310 nm attributed to the π–π^* transition of aromatic C=C bonds, which indicative of a large π-conjugation network within the IL-RGO and S-RGO. The relationship between the absorbance intensity and the bilayer number shown in Fig. 4e further suggests that almost the same amount of IL-RGO and S-RGO has been loaded in each assembling step and a regular and uniform multilayer films has been constructed.

3.3. Electrochemical behavior of $\{$IL-RGO/S-RGO$\}_n$ films toward H_2O_2

The electrocatalytic activity of $\{$IL-RGO/S-RGO$\}_n$ films was investigated taking H_2O_2 as the probe firstly. Fig. 5A illustrates the cyclic voltammograms (CV) for $\{$IL-RGO/S-RGO$\}_5$ modified electrode in PBS (pH 7.4) solutions without (a) and with (b) 10 mM H_2O_2 at the scan rate of 200 mV s^{-1}. It can be seen that the cathodic current begins to rise at 0.2 V in PBS with 10 mM H_2O_2 compared to that in PBS without H_2O_2, which shows excellent reduction toward H_2O_2 of the $\{$IL-RGO/S-RGO$\}_5$ films. By changing the bilayer number of the $\{$IL-RGO/S-RGO$\}_n$ multilayer film, it is possible to tune the electrocatalytic activity toward H_2O_2.

The dependence of amperometric responses of $\{$IL-RGO/S-RGO$\}_5$ biosensor toward 5 mM H_2O_2 on different operating

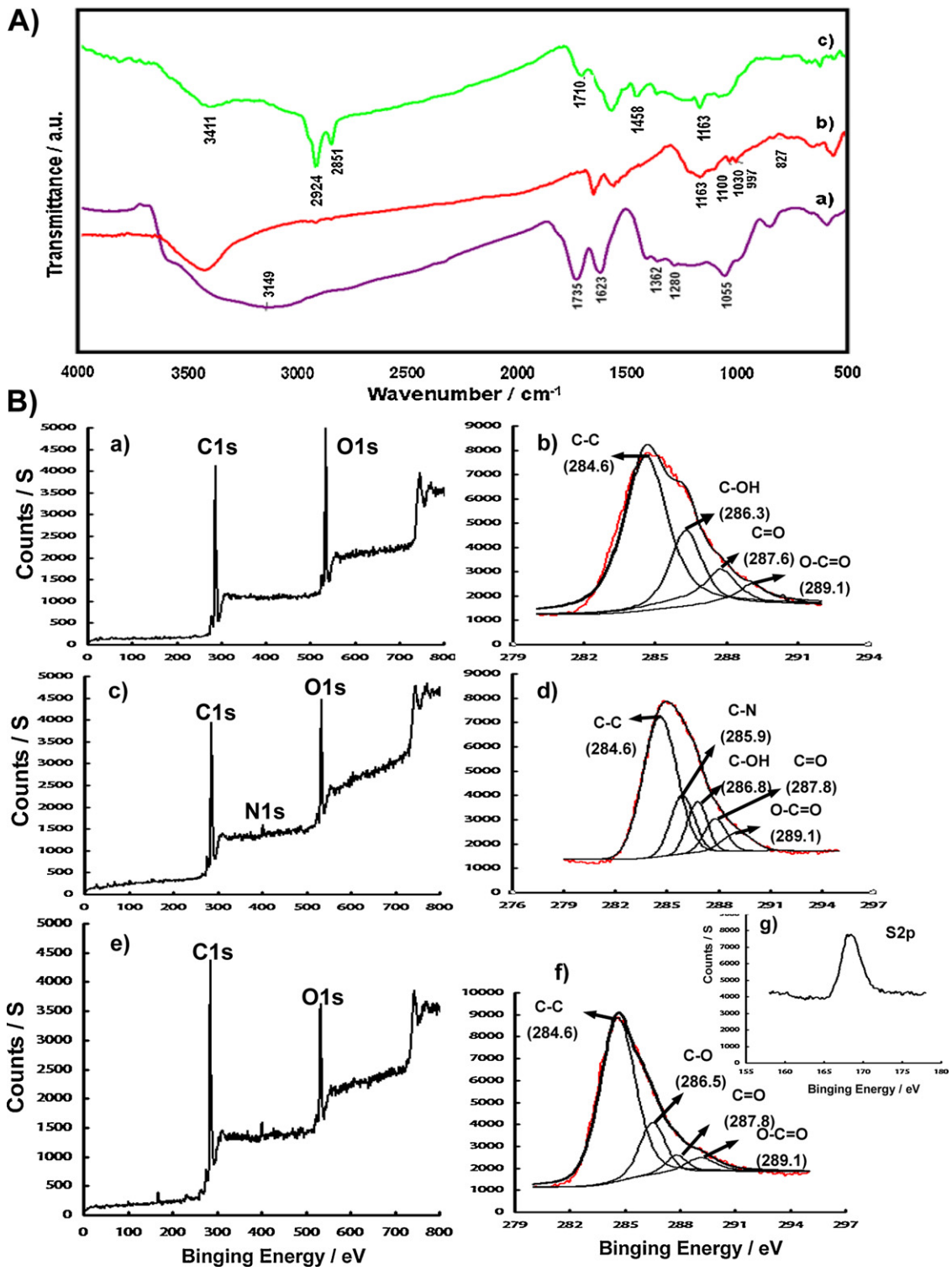

Fig. 3. (A) FTIR spectra of GO (a), S-RGO (b), IL-RGO(c). (B) Survey XPS data for GO (a), IL-RGO (c) and S-RGO (e), high-resolution C1s spectra of the GO (b), IL-RGO (d) and S-RGO (f) and high-resolution XPS S 2p spectra of S-RGO (g) showing evidence of a sulfonic group.

potentials was also investigated and shown in Fig. 5B. The currents were measured point by point at each potential from −100 mV to −350 mV. As shown in Fig. 5B, the amperometric responses increase slightly when the potential ranges from −100 mV to −200 mV and then rises sharply from −200 mV to −350 mV. Considering the noise of the background and the interferences from oxygen and AA, −200 mV was selected as the optimal working potential and used in the following electrochemical experiments.

Fig. 5C shows the dependence of the reduction current on the number of bilayers. The current value increases slightly in the first three bilayers, after which the growth speeds up and reaches the maximum at the fifth bilayer. With the increasing number of the graphene, the electroactive area of the electrode is larger, which can effectively improve the sensitivity of the detection of H_2O_2, and reach the maximum at five bilayer. However, further increase in the bilayer could only lead to an obvious decrease in the

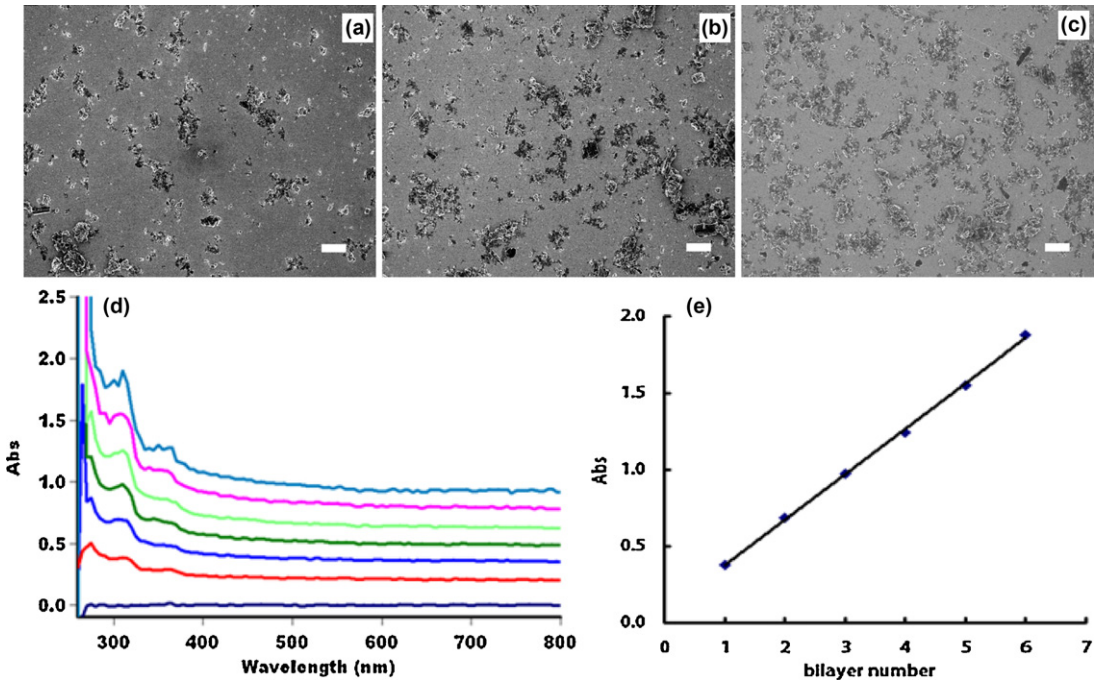

Fig. 4. SEM images of the films of one bilayer (a), two bilayers (b) and three bilayers (c). All scale bars shown represent 500 nm. UV–vis-NIR absorption spectra of {IL-RGO/S-RGO}$_n$ (n = 1–6) multilayer films assembled on a quartz slide (d). A plot of the absorption at 310 nm *versus* the bilayer number (e).

reduction current, which was induced by the so thicker film that blocks the electron transfer from the substrate to the electrode. Thus, {IL-RGO/S-RGO}$_5$ multilayer films was selected as the optimal film and used in the following electrochemical experiments.

Fig. 5D illustrates the typical amperometric responses with successive additions of H_2O_2. The inset of Fig. 5D depicts the relationship between the increment in reduction peak current of {IL-RGO/S-RGO}$_5$ biosensor and the concentration of H_2O_2. As shown, the peak currents increase linearly with the concentration of H_2O_2 ranging from 0.1 to 3.4 mM (I (μA) = 0.1364C (mM) + 0.0318) with a correlation coefficient of 0.9953 and a sensitivity of 0.1364 ± 0.0054 μA μM^{-1}. The detection limit, based on the signal-to-noise ratio of three, was calculated to be 0.21 μM.

3.4. In vitro measurement of glucose with on-line microdialysis system

The reduction current of glucose was calibrated *in vitro* with known concentrations of glucose before the *in vivo* experiments. Fig. 6 is the current responses of different concentrations of glucose with the on-line microdialysis system *in vitro* at the perfusion rate of 2.0 μL/min. Well-defined steady-state currents are obtained for standard glucose solutions which are continuously injected into the on-line microdialysis system. The current responses were in good linear with glucose from 10 μM to 500 μM (I (nA) = 0.0718C (μM) + 0.9875, γ = 0.9922) with a sensitivity of 0.0718 ± 0.00648 nA μM^{-1}. The detection limit, based on the signal-to-noise ratio of three, was calculated to be 3.33 μM. This result was much lower than those obtained at graphene-CdS nanocomposite (Wang et al., 2010), self-assembled graphene platelet modified (Liu et al., 2011) and graphene-chitosan modified glucose biosensors (Kang et al., 2009).

The apparent Michaelis–Menten constant ((*K*app m), which is an indication of enzyme–substrate kinetics, can be calculated according to the Lineweaver–Burk equation (Kamin and Wilson, 1980). In this work, when the concentration of glucose was from 10 μM to 500 μM, the K_m^{app} value was about 0.325 mM, much smaller than previous relative reports of 2.59 mM (Yang et al., 2009a,b) and 1.57 mM (Pradhan et al., 2010). Since the smaller K_m^{app} shows the higher catalytic ability, we can conclude that the {IL-RGO/S-RGO}$_5$/GOx/Nafion biosensor displays a higher affinity and enzymatic activity in the range of lower concentration of glucose.

3.5. Selectivity of the {IL-RGO/S-RGO}$_5$/GOx/Nafion biosensor with the microdialysis system

Ascorbic acid (AA), dopamine (DA) and uric acid (UA), present in physiological fluids, are considered to be the most important interferences for direct electrochemical reduction of glucose due to their high concentrations in biological samples (Lu et al., 2011; Yu et al., 2011a,b). In the present work, the selectivity of {IL-RGO/S-RGO}$_5$/GOx/Nafion biosensor for the detection of glucose was evaluated with the on-line microdialysis system. Fig. S1A displays on-line amperometric responses for 0.1 mM AA, 10 μM DA, 50 μM UA and 100 μM, 50 μM, 20 μM glucose at the working potential of −200 mV. The result shows that 0.1 mM AA, 10 μM DA and 50 μM UA cannot produce measurable current responses, which indicates that the measurement of glucose are essentially interference-free from these electroactive species. Therefore, the low operating potential, combining with the use of "artificial peroxidase" to replace "natural peroxidase" in the present work offers a selective electrochemical method for on-line measurements of biological compounds with *in vivo* microdialysis.

3.6. Reproducibility and stability of the {IL-RGO/S-RGO}$_5$/GOx/Nafion biosensor with the on-line microdialysis system

The reproducibility of the method was estimated through consecutively measuring glucose (100 μM) at the {IL-RGO/S-RGO}$_5$/GOx/Nafion modified electrode with the microdialysis system for 5 times shown in Figure S1B. The RSD value for the

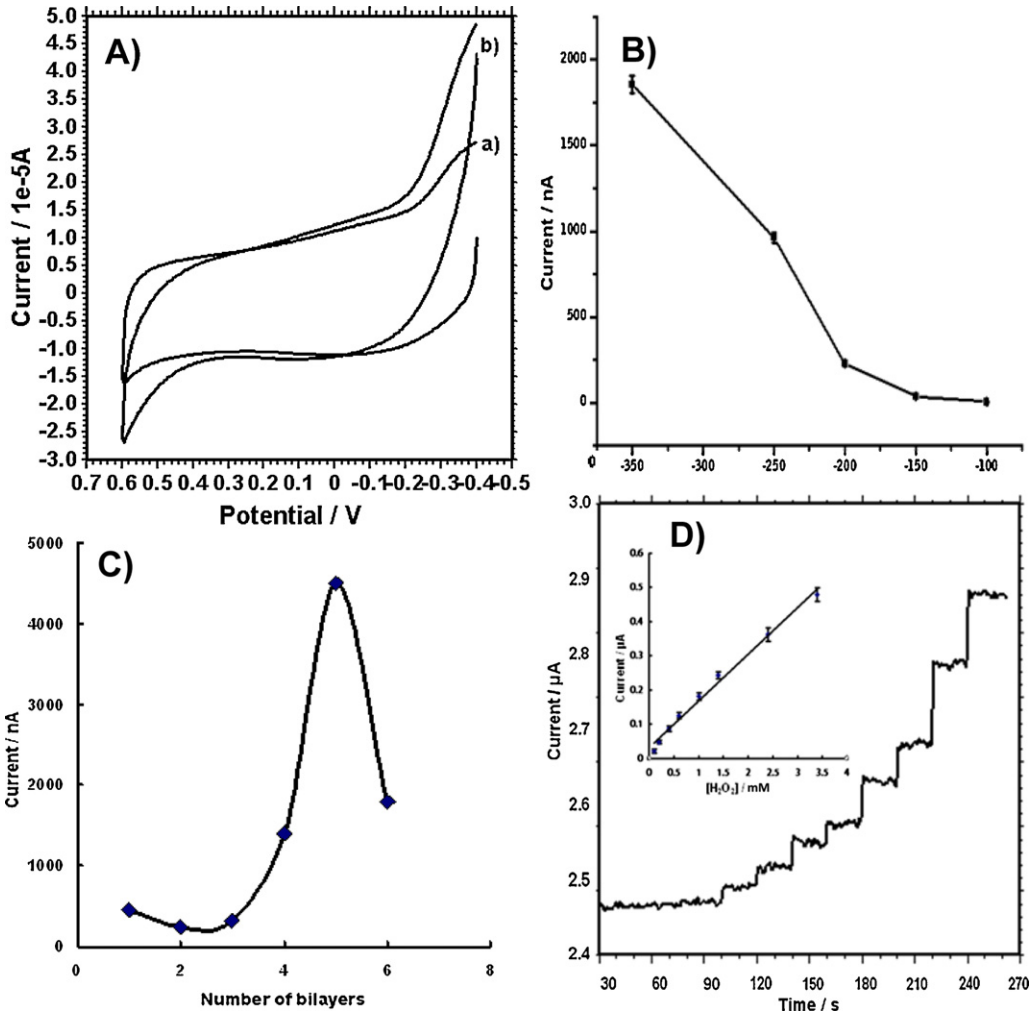

Fig. 5. (A) cyclic voltammograms of $\{IL\text{-}RGO/S\text{-}RGO\}_5$ modified electrode in PBS solution (pH 7.4) without (a) and with 10 mM H_2O_2 (b). (B) dependence of the responses of $\{IL\text{-}RGO/S\text{-}RGO\}_5$ modified electrode to 5 mM H_2O_2 on different working potentials from −300 mV to −100 mV. (C) dependence of the responses of the electrode modified with $\{IL\text{-}RGO/S\text{-}RGO\}_n$ (n = 1–6) to 5 mM H_2O_2. (D) Amperometric responses of $\{IL\text{-}RGO/S\text{-}RGO\}_5$ biosensor toward different standard solutions of H_2O_2. Inset shows the calibration curve for H_2O_2 from 0.1 mM to 3.4 mM.

amperometric currents (n = 5) was calculated to be 3.9%, indicating an acceptable fabrication reproducibility under the mentioned conditions.

The stability of the $\{IL\text{-}RGO/S\text{-}RGO\}_5$/Gox/Nafion biosensor was checked by employing the biosensor with the on-line microdialysis system for at least 6 days (5–6 h each day). The RSD of current responses to 100 μM glucose decreased about 4.8%. Moreover, the biosensor retained almost 83% of their initial activity after they were stored at +4 °C for two weeks. The good long-term stability can be ascribed to the excellent biocompatibility of the $\{IL\text{-}RGO/S\text{-}RGO\}_5$ films, which provides a favorable microenvironment for GOx to maintain its bioactivity.

3.7. Basal level and variation of glucose concentration in rat's striatum following insulin injection

After the continuous perfusion for 90 min with aCSF solution, the on-line microdialysis system can start to measure glucose as section 2.4 depicted. The relative recovery for glucose was calculated to be 24% at the flow rate of 2.0 μL/min. For the determination of relative recovery, the probe was immersed in a vial filled with a known concentration of glucose and then the probe was perfused with aCSF solution at the rate of 2.0 μL/min. The relative recovery is just the ratio between the concentration of glucose which can be calculated from its calibration curve and the known concentration of glucose in the vial. It can be calculated from the following equation:

$$R(\%) = \frac{C_{out}}{C_{in}} \times 100$$

where $R(\%)$ is the relative recovery in percentage, C_{out} is the concentration of the solution calculated from the calibration curve, C_{in} is the known concentration of the solution in the vial. Fig. 6B displays typical amperometric responses for the microdialysates continuously sampled from the rat's striatum. There were three rats that were totally investigated. Based on our postcalibration, the basal glucose concentration in the striatum of rat was calculated to be 0.376 ± 0.028 mM (mean ± s.d., n = 3), which is comparable to those previously reported using on-line microdialysis (Lin et al., 2007, 2009).

Moreover, to investigate whether the biosensor was capable of detecting dynamic change of glucose in the rat brain, the influence of exogenous substance administration was studied in this work. Fig. 6B shows the variation of glucose concentration in the striatum of rat following the injection (i.p.) of 30 μL insulin. As can be seen, the current responses of the dialysate with

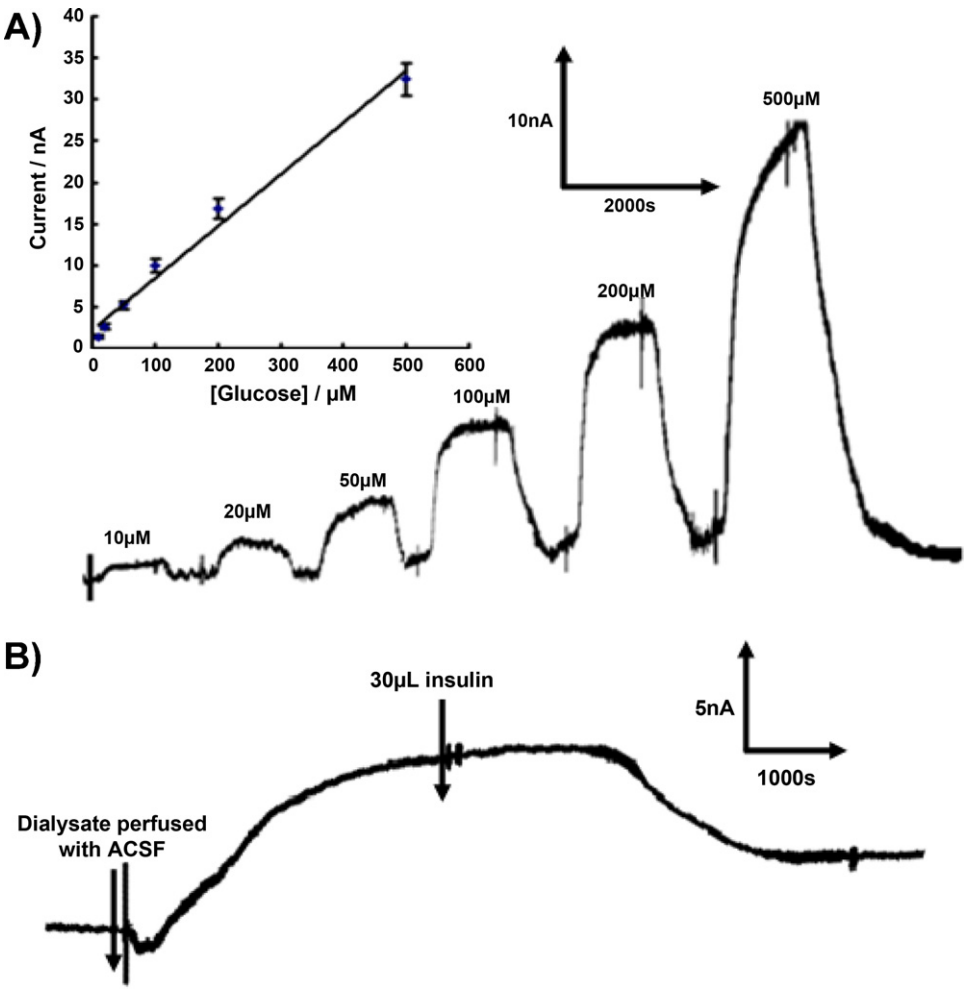

Fig. 6. (A) Amperometric responses of $\{IL\text{-}RGO/S\text{-}RGO\}_5$/GOx/Nafion biosensor toward different standard solutions of glucose in on-line microdialysis system. Inset shows the calibration curve for glucose from 10 μM to 500 μM. (B) Current-time plots of $\{IL\text{-}RGO/S\text{-}RGO\}_5$/GOx/Nafion biosensor on brain dialysate from the striatum of anesthetic rats and rats stimulated by injection (i.p.) of 30 μL insulin.

$\{IL\text{-}RGO/S\text{-}RGO\}_5$/GOx/Nafion biosensor starts to decrease after insulin injection for an average of 34.68 min ($n = 3$). This tendency lasts about 25 min until the current reaches a minimum. After calibration, the glucose level in the rat striatum has declined to be $52.75 \pm 8.6\%$ (mean ± s.d., $n = 3$) of the basal level after the administration of 30 μL insulin. These above results indicate that the $\{IL\text{-}RGO/S\text{-}RGO\}_5$ based enzymatic biosensor developed here could be applied to various neurophysiological studies, including the real-time change in the neurotransmitter release or uptake.

4. Conclusions

A new composite material $\{IL\text{-}RGO/S\text{-}RGO\}_n$ were self-assembled through the layer-by-layer (LBL) method herein and a novel glucose biosensor based upon $\{IL\text{-}RGO/S\text{-}RGO\}_5$ films was constructed. By efficiently integrating *in vivo* microdialysis sampling and online selective electrochemical detection, we have successfully continuous *in vivo* detected glucose in the rat brain based on the new fabricated sensor. Both the normal level and variation of glucose concentration in the striatum of rats following insulin stimulations were successfully observed. In addition to the good linearity, stability and high selectivity of this sensor, $\{IL\text{-}RGO/S\text{-}RGO\}_5$ modified sensor with its low working potential, is well suitable for further research *in vivo*.

Acknowledgements

This work is supported by the National Natural Science Foundation of China (No. 21175044) and the Programs of the Science & Technology Commission of Shanghai Municipality (10JC1404000 and 10JC1411200). We also greatly thank the Fundamental Research Funds for the Central Universities and the Research Fund for the Doctoral Program of Higher Education (20100076110002).

Appendix A. Supplementary data

Supplementary data associated with this article can be found, in the online version, at doi:10.1016/j.bios.2011.11.044.

References

Allen, M.J., Tung, V.C., Kaner, R.B., 2010. Chem. Rev. 110, 132–145.
An, X., Simmons, T., Shah, R., Wolfe, C., Lewis, K.M., Washington, M., Nayak, S.K., Talapatra, S., Kar, S., 2010. Nano Lett. 10, 4295–4301.
Bai, H., Li, C., Shi, G., 2011. Adv. Mater. 23, 1089–1115.
Berger, C., Song, Z.M., Li, X.B., Wu, X.S., Brown, N., Naud, C., Mayou, D., Li, T.B., Hass, J., Marchenkov, A.N., Conrad, E.H., First, P.N., Heer, W.A., 2006. Science 312, 1191–1196.
Cataldo, F., 2003. Fuller Nanotubes Car. N 11 (1), 1–13.
Guo, S., Dong, S., Wang, E., 2010. ACS Nano 4, 547–555.
Kamin, R.A., Wilson, G.S., 1980. Anal. Chem. 52, 1198–1205.
Kong, B.-S., Geng, J., Jung, H.-T., 2009. Chem. Commun., 2174–2176.

Kosynkin, D.V., Higginbotham, A.L., Sinitskii, A., Lomeda, J.R., Dimiev, A., Price, B.K., Tour, J.M., 2009. Nature 458, 872–876.
Kou, R., Shao, Y., Wang, D., Engelhard, M.H., Kwak, J.H., Wang, J., Viswanathan, V.V., Wanga, C., Lin, Y., Wanga, Y., Aksay, I.A., Liu, J., 2009. Electrochem. Commun. 11, 954–957.
Lee, C., Wei, X., Kysar, J.W., Hone, 2008. J. Sci. 321, 385–388.
Li, D., Müller, M.B., Gilje, S., Kaner, R.B., Wallace, G.G., 2008. Nat. Nanotechnol. 3, 101–105.
Li, X., Cai, W., An, J., Kim, S., Nah, J., Yang, D., Piner, R., Velamakanni, A., Jung, I., Tutuc, E., Banerjee, S.K., Colombo, L., Ruoff, R.S., 2009. Science 324, 1312–1314.
Lin, Y., Liu, K., Yu, P., Xiang, L., Li, X., Mao, L., 2007. Anal. Chem. 79, 9577–9583.
Lin, Y., Zhu, N., Yu, P., Su, L., Mao, L., 2009. Anal. Chem. 81, 2067–2074.
Liu, L.-H., Yan, M., 2009. Nano Lett. 9, 3375–3378.
Liu, J., Bai, H., Wang, Y., Liu, Z., Zhang, X., Sun, D.D., 2010. Adv. Funct. Mater. 20, 4175–4181.
Liu, S., Tian, J., Wang, L., Luo, Y., Lu, W., Sun, X., 2011. Biosens. Bioelectron. 26, 4491–4496.
Lu, L., Li, H.B., Qu, F., Zhang, X.B., Shen, G.L., Yu, R.Q., 2011. Biosens. Bioelectron. 26, 3500–3504.
Muszynski, R., Seger, B., Kamat, P.V., 2008. J. Phys. Chem. C 112, 5232–5238.
Niyogi, S., Bekyarova, E., Itkis, M.E., McWilliams, J.L., Hamon, M.A., Haddon, R.C., 2006. J. Am. Chem. Soc. 128, 7720–7721.
Park, J.S., Cho, S.M., Kim, W.-J., Park, J., Yoo, P.J., 2011. Appl. Mater. Interfaces 3 (2), 360–368.
Pradhan, D., Niroui, F., Leung, K.T., 2010. Appl. Mater. Interfaces 2 (8), 2409–2412.
Reina, A., Jia, X.T., Ho, J., Nezich, D., Son, H.B., Bulovic, V., Dresselhaus, M.S., Kong, J., 2009. Nano Lett. 9, 30–35.
Shan, C., Yang, H., Han, D., Zhang, Q., Ivaska, R., Niu, L., 2009. Langmuir 25 (20), 12030–12033.
Shi, G.Y., Yamamoto, K., Zhou, T.S., Xu, F., Kato, T., Jin, J.Y., Jin, L.T., 2003. Electrophoresis 24, 3266–3272.
Si, Y., Samulski, E.T., 2008. Nano Lett. 8, 1679–1682.
Stankovich, S., Dikin, D.A., Dommett, G.H.B., Kohlhaas, K.M., Zimney, E.J., Stach, E.A., Piner, R.D., Nguyen, S.T., Ruoff, R.S., 2006a. Nature 442, 282–286.
Stankovich, S., Piner, R.D., Nguyen, S.T., Ruoff, R.S., 2006b. Carbon 44, 3342–3347.
Stoller, M.D., Park, S.J., Zhu, Y.W., An, J.H., Ruoff, R.S., 2008. Nano Lett. 8, 3498–3502.
Subbiah, A., Liu, C., Ashok Kumar, Li, C.-Z., 2010. J. Phys. Chem. C 114, 12920–12924.
Szabo, T., Berkesi, O., 2005. Carbon 43 (15), 3186–3189.
Tung, V.C., Allen, M.J., Yang, Y., Kaner, R.B., 2009. Nat. Nanotechnol. 4, 25–29.
Wang, K., Liu, Q., Guan, Q.-M., Wu, J., Li, H.-N., Yan, J.-J., 2010. Biosens. Bioelectron. 26, 2252–2257.
Kang, X., Wang, J., Wa, H., Aksayc, I.A., Liu, J., Lin, Y., 2009. Biosens. Bioelectron. 25, 901–905.
Xu, Y., Bai, H., Lu, G., Li, C., Shi, G., 2008. J. Am. Chem. Soc. 130, 5856–5857.
Yang, H., Shan, C., Li, F., Han, D., Zhang, Q., Niu, L., 2009a. Chem. Commun. 26, 3880–3882.
Yang, K., She, G.-W., Wang, H., Ou, X.-M., Zhang, X.-H., Le, C.-S., Lee, S.-T., 2009b. J. Phys. Chem. C 113, 20169–20172.
Yu, D., Dai, L., 2010. J. Phys. Chem. Lett. 1, 467–470.
Yu, Y., Liu, X., Jiang, D., Sun, Q., Zhou, T., Zhu, M., Jin, L., Shi, G., 2011a. Biosens. Bioelectron. 26, 3227–3232.
Yu, Y., Sun, Q., Zhou, T., Zhu, M., Jin, L., Shi, G., 2011b. Bioeletrochemistry 81, 53–57.
Zeng, Q., Cheng, J.S., Tang, L.H., Liu, X.F., Liu, Y.Z., Li, J.H., Jiang, J.H., 2010. Adv. Funct. Mater. 20, 3366–3372.
Zhang, Y.H., Tang, Z.R., Fu, X.Z., Xu, Y.J., 2010. ACS Nano 4, 7303–7314.
Zhang, Q., Wu, S., Zhang, L., Lu, J., Verproot, F., Liu, Y., Xing, Z., Li, J., Song, X.-M., 2011. Biosens. Bioelectron. 26, 2632–2637.
Zhu, Y., Tour, J.M., 2010. Nano Lett. 10 (11), 4356–4362.
Zhou, M., Zhai, Y., Dong, S., 2009. Anal. Chem. 81 (14), 5603–5613.